CHAPTER 33

MEASUREMENT OF DIRECT-CONTACT CONDENSATION OF SATURATED VAPOR ON SUBCOOLED DROPLETS BY PULSED LASER HOLOGRAPHY

Anseimo Chávez, Peter Gebhard and Franz Mayinger

1. INTRODUCTION

Condensation of vapor on spray droplets has recently been investigated in several detailed studies [1-4]. The reason for the interest lies in the numerous applications of sprays in many fields of the chemical industries and power engineering.

Here we investigate the growth rate of subcooled droplets injected into saturated vapor of the same substance by applying pulsed laser holography. Taking single and double pulsed holograms of the spray droplets at steady-state conditions, it is possible to measure increments in droplet size caused by the condensation of the vapor. Single pulsed holograms supply information about position, distribution and concentration of the droplets in the injection volume. Double pulsed (i.e. double exposure) holograms also provide information about the velocity distribution of the droplets, which is necessary for the computation of the residence time in the volume of interest.

The aim of this report is to describe an approach to the automated evaluation of pulsed laser holograms of sprays. The holograms to be evaluated are of the "off-axis" type as can be obtained from the holographic arrangement presented in Fig. 1. They contain information about size, position and velocity of the spray droplets and about the form of the spray cone. The spray is produced by injecting subcooled liquid of the refrigerant R113 into an environment formed by its own saturated vapor.

The spray flow of the liquid refrigerant R113 used as a model fluid corresponds to droplet Reynolds numbers in the range of $100 \leq Re \leq 3500$. The pressure of the vapor environment is varied in a range of reduced pressures of $0.03 \leq p_r \leq 0.3$, which is one order of magnitude greater than in other studies reported. A pressure swirl nozzle (∅ 0.6 mm, 60°) of the hollow-cone type which produces drops of size D in the range of $30 \leq D \leq 300$ µm is used as an atomizer. The results of this investigation are not only useful for spray characterization but also for the design of heat exchange equipment and detailed explanation of the transport process. Moreover, they are suitable to estimate the behavior of thermally based injection processes in agricultural applications.

Special emphasis is given to the discussion of our technique developed to scan the holographic image, the criterion adopted to select well-focussed droplets and, in the case of double pulsed

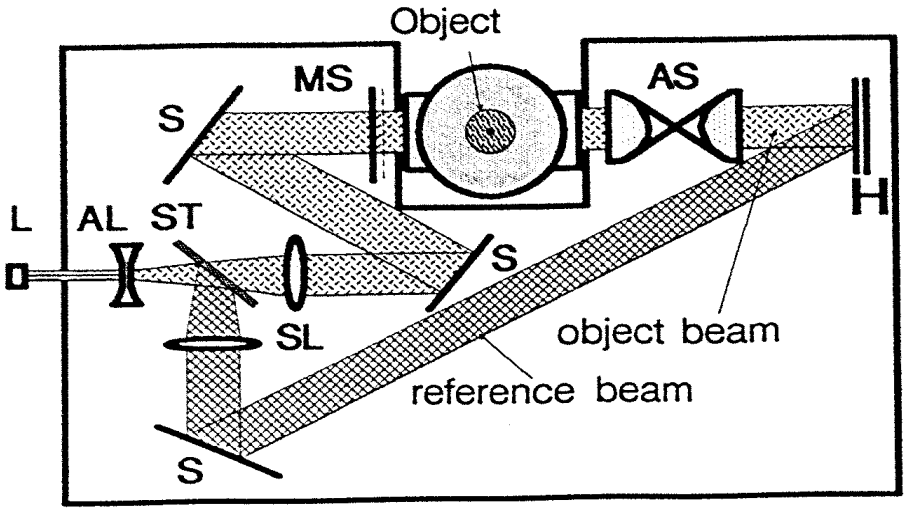

Figure 1: Optical arrangement of the holocamera.

holograms, to identify those spot pairs in the scanned image corresponding to droplets imaged at two successive positions by double exposure of the same holographic plate. The results of evaluating of a series of 160 pulsed holograms of the R113 spray at different injection mass flow rates (0.8, 1.37, 2.0, 2.72, 3.86 g/s) and vapor pressures (0.1 – 1.0 MPa) are included.

2. OPTICAL SET-UP AND EXPERIMENTAL CHAMBER

2.1 Holographic Technique

The pulsed laser holography represents one of the more suitable noninvasive measurement methods for the study of transport phenomena (e.g. heat and mass transfer) in dispersed transparent flows. It provides three dimensional (3D) scenes of the volume of interest taken at a very short exposure time (~30 ns). The recorded holograms can be reconstructed with help of a continuous laser beam. Figure 1 shows the optical set-up for the recording of off-axis holograms. Using a separate reference beam, the holographic reconstructions can be observed directly, or with help of a microscope as in a photograph. The resulting reconstructed images are very clear for particle sizes $d > 10\lambda$ where D and λ are the drop diameter and the wavelength of the laser light used to record the hologram, respectively. Position and velocity of the particles of the dispersed phase can also be obtained from the reconstructions. The principal features of the method and some advanced adaptations are explained in detail by Trollinger [5] and Chávez and Mayinger [6].

3.2 Experimental Chamber

Figure 2 shows a scheme of the experimental chamber. It consists of a thermally insulated cylindrical autoclave of 206 mm inner diameter and 650 mm in height, designed for pressures up to 2 MPa. Two quartz glass windows (ϕ 100 mm) installed in the cylindrical wall provide the optical access. The liquid is injected from the top of the vessel through the hollow cone

nozzle. The nozzle, concentric with respect to the cylindrical wall, can axially be moved to permit the observation of any section of the spray. The lower third of the vessel is filled with liquid refrigerant R113 which is heated by an electrical resistance (1.2 kW) installed on the lower plenum, to produce the saturated vapor environment in the injection space of the autoclave. A funnel is placed between the boiling liquid and the spray to collect the spray droplets and lead them to the outlet.

Measurements of temperature and pressure at different points of interest in the facility were carried out with conventional thermocouples and pressure sensors monitored by a personal computer.

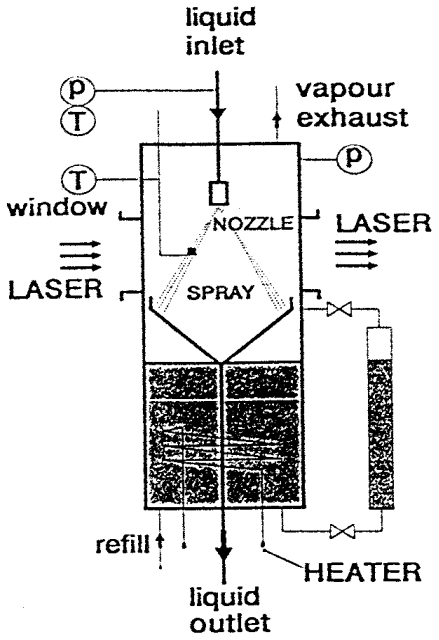

Figure 2: Experimental facility.

3. IMAGE PROCESSING OF HOLOGRAPHIC RECONSTRUCTIONS

The principal problem in the application of pulsed laser holography lies in handling the large amount of information contained in the holograms. One single hologram can store information about position, size, and velocity of many thousands of droplets. Comprehensive studies of the characteristics of the droplets and their interactions with the gaseous environment necessarily require the help of computer–aided particle counting and measuring methods. Fortunately, the rapid development of the computer technology in the last years, as well as the miniaturization and mass production of computer components, has made many applications of the digital analysis and processing of images possible.

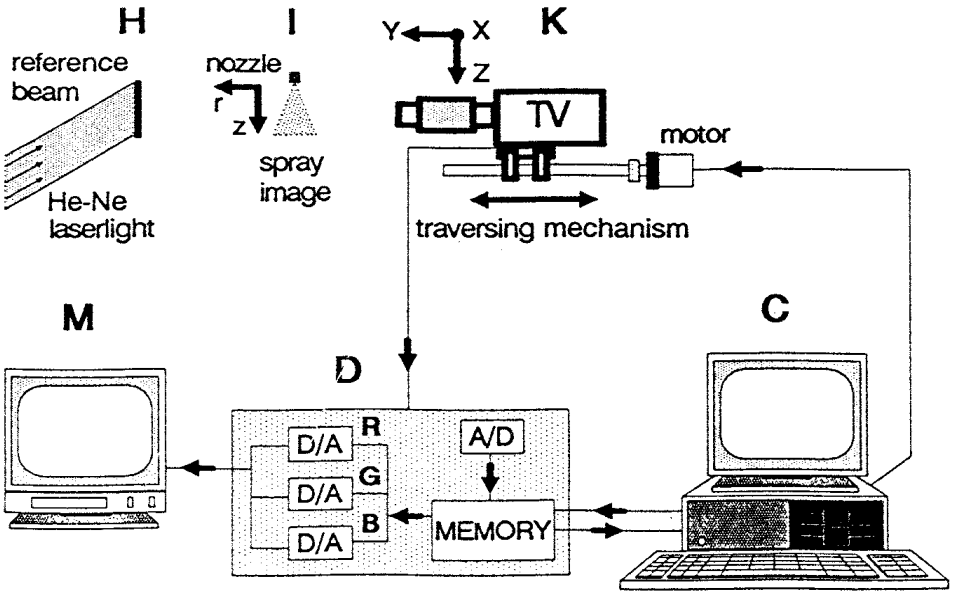

Figure 3: Digital image processing system.

3.1 Image Processing System

The components of the digital image processing system are shown in the flow diagram of Fig. 3. The hologram **H** is reconstructed by illumination with a continuous parallel beam from a He–Ne–laser, which simulates the reference beam. The optical information contained in the reconstructed image **I** is scanned by the video camera **K**, and transmitted to the digitizer **D**. Here, the signal is transformed into digital information and is stored in the frame memory of the digitizer, in form of an array of 512 x 512 picture elements (pixels) of 8 bits. This means that each picture appears as a pixel matrix in which the color of each pixel can be represented by one of 2^8 possible grey tones. The digitizer is directly connected to the host computer **C** by a 16 bit bus interface, allowing for fast communication. The processing of the digitized picture is then carried out by the host computer using the digitizer frame memory interactively, for pixel allocation. In order to visualize the information actually stored in the digitizer frame memory, this produces a continuous RGB (false color: red, green, blue) output signal which can be observed on the graphics monitor **M**.

3.2 Scanning of Holographic Images

The pictures to be scanned are obtained from single or double pulsed holograms. They represent a three–dimensional (3–D) image corresponding to a "frozen" scene of the spray, as shown in the scheme of Fig. 4. In this scheme, **r** and **z** are axis symmetrical, cylindrical coordinates with origin **O** at the nozzle outlet. Single pulsed holograms contain information about the geometry of the spray, the break–up of the liquid sheet, and the droplet distribution in the control volume. Complementary, double pulsed holograms provide information about the droplet velocities and trajectories. Due to the fact that the video camera can only record two–dimensional (2–D) pictures, for example in the optical plane **X–Z**, it must be focussed stepwise along the depth coordinate **Y** in order to process the 3–D holographic image, as suggested in Fig. 4. In this manner, the 3–D holographic image is transformed into a series of many 2–D video pictures.

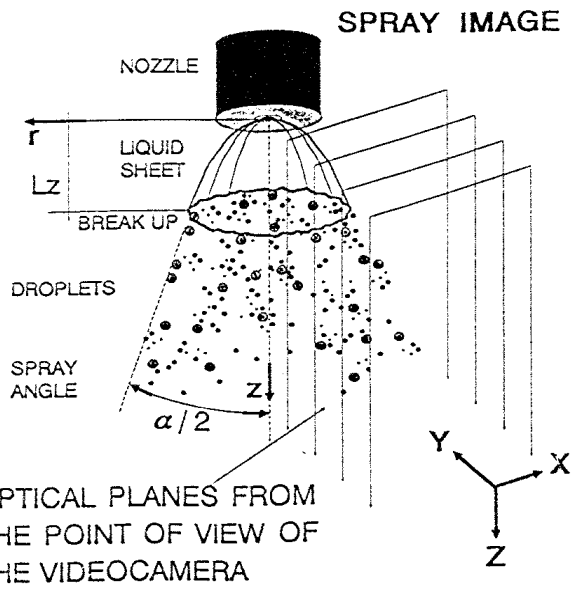

Figure 4: Description of a spray flow and the scanning of holographic reconstruction by a videocamera.

In order to control the position of the camera and to measure the values of the **Y**–coordinate, the camera was mounted on a traversing mechanism (as schematically indicated in Fig. 3).

4. EVALUATION ROUTINES

The images to be processed contain a collection of spots of different grey–values, ranging from 0 = black to 255 = white, representing the spray droplets, and a given fine grain pattern forming a noisy background (speckle noise). This speckle pattern is produced by the diffuse, coherent illumination used to record the hologram.

Although single and double pulsed holograms are of the same nature and their evaluation is similar, we decided to configure two different evaluation routines: the routine EINZEL, evaluating single pulsed holographic images for which accurate measurements of the drop size are of essential importance, and the routine DOPPEL, which evaluates the images obtained from double pulsed holograms. For this later case, the size of the droplets does not need to be recalculated; the routine DOPPEL is dedicated to identify spot couples which are originated by droplets imaged at two successive positions. The distance between these successive positions represents the droplet velocity.

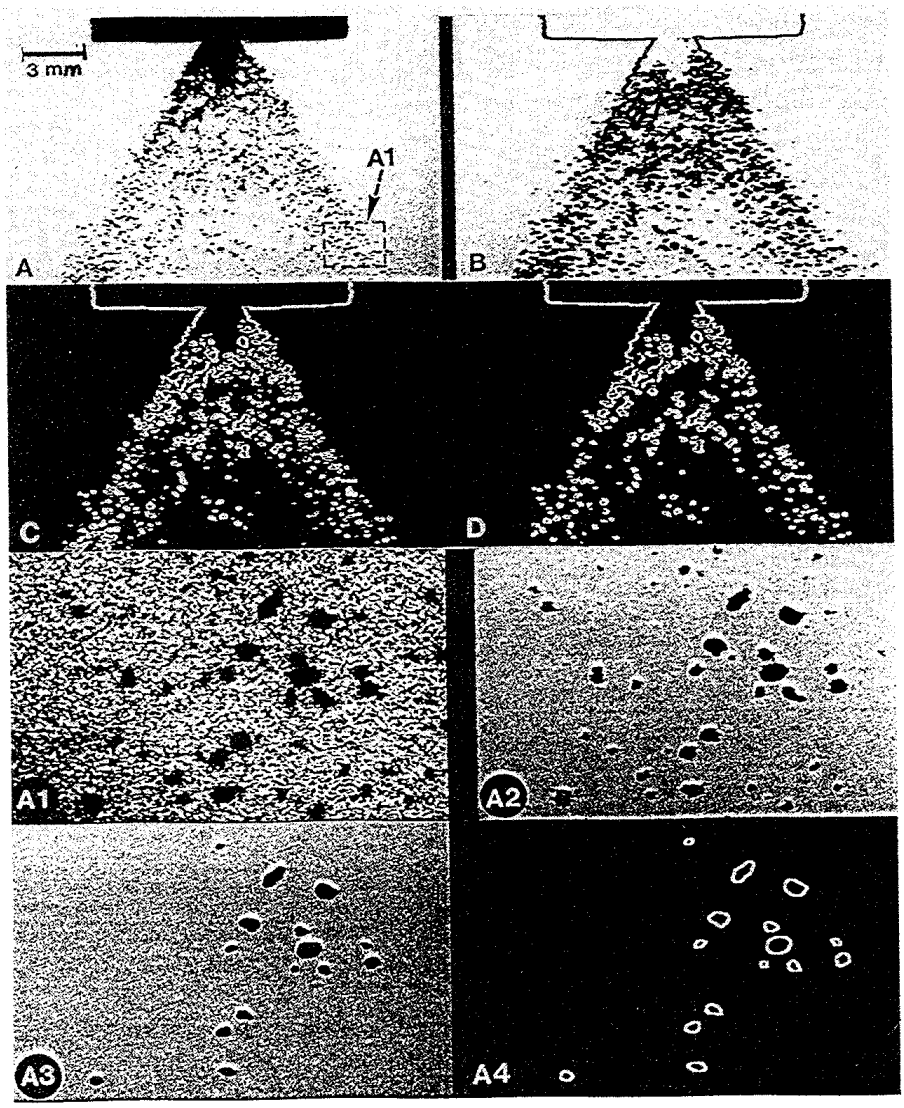

Figure 5: *Representative steps of the image processing of a single pulsed hologram of the R113 spray. A) Original image, B) and C) smoothing gradient extraction, contouring and D) binarization. The lower pictures depict the enlarged droplet zone of picture (A), its noise filtering and the final droplet identification.*

4.1 The EINZEL Routine

The processing of images obtained from single pulsed holograms involves the separation of the droplet images from the background, the identification of the sharp focussed droplets, measuring their projected areas, and the evaluation of their equivalent diameters and center points with respect to a reference frame. All these operations, from the image capture by the video camera to the final result, are carried out by the program EINZEL. It consists of a series of digital filters and gradient operators selected from standard image processing libraries and our own algorithms developed for measuring, calibrating and data handling.

Examples of representative stages of the image processing are presented in form of photographs in Fig. 5. Here, photographs A to D show the focussing process. The contour of the nozzle is sketched for better orientation. A represents an original view from the holographic reconstruction, B the gradient extraction, C contouring and D the binarization. Enlargements A1–A4 of the droplet zone of Fig. 5A illustrate the process of noise filtering and the final result.

To assure high confidence in the measurement, our method was calibrated by evaluating a hologram of glass pearls which were previously measured with the help of a microscope. The pearl images were measured at different enlargements. For each enlargement, the pixel size was calibrated by using an optical grid. As expected, the binary pearl images represented by 6 to 10 pixels presented relative large deviations of the order of 7% with respect to their calibrated size. For image representations with 40 or more pixels, the deviation was smaller than 1%.

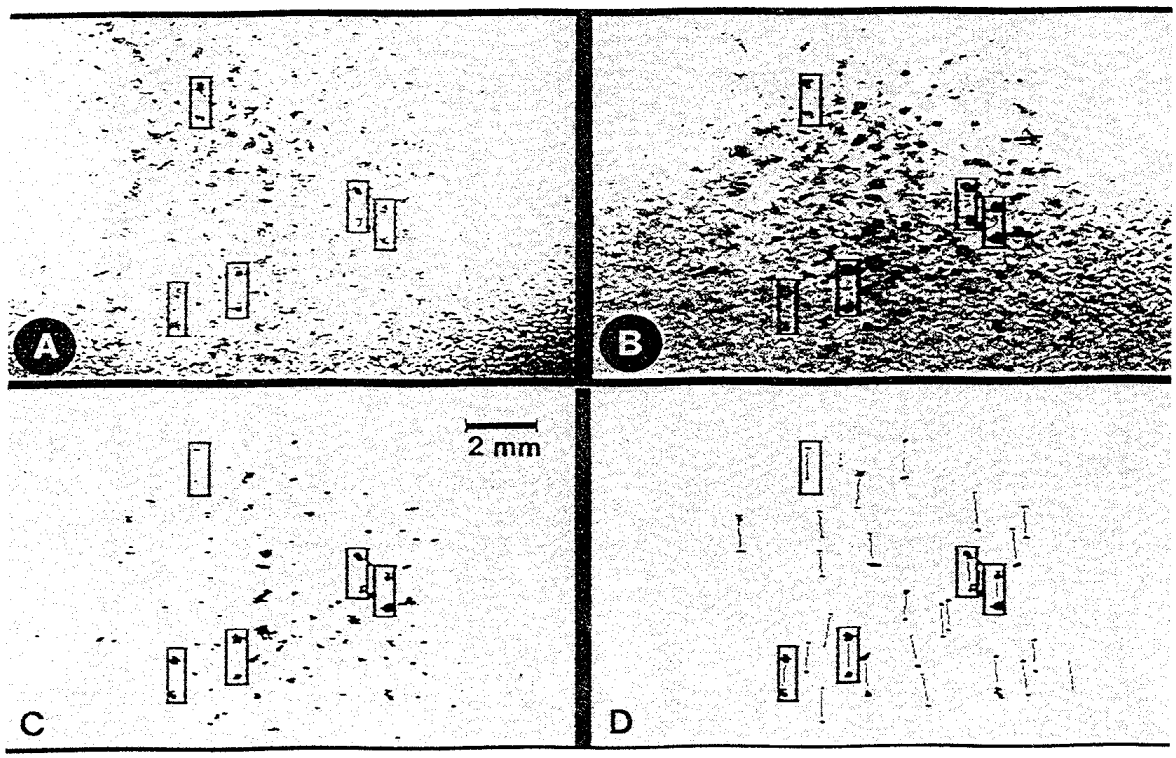

Figure 6: Evaluation of a double pulsed hologram.

4.2 The DOPPEL Routine

From double-pulsed holograms one obtains information about velocities and trajectories of the droplets. The holograms represent a conglomeration of spot couples, in which each couple represents a spray droplet imaged at two successive positions corresponding to the time interval (1–800 μs) between the two exposures used to record the hologram. In order to evaluate the double-pulsed images, the routine DOPPEL was developed. The task of the program DOPPEL consists in identifying the spot couples from the pictures taken by the video camera, in measuring the distance between the center points of the two successive droplet images, and in computing the droplet trajectories related to the space coordinates in the injection volume. Representative stages of the image processing are presented in form of photographs in Fig. 6. In this figure, A represents the source image, B the fuzzy mask, C the image after noise filtering, D the identification of spot couples and the evaluation of the image.

In order to find the velocities and the trajectories in a reconstruction of a double pulsed hologram, the subroutine VEL was developed. It consists of two modules: a spatial frequency analyzer and a measuring algorithm. For the description of the subroutine performance, the photograph A of Fig. 7 will be analyzed. Without regard to color or form and with the previous assumption that Fig. 7A was obtained from a double pulsed holographic reconstruction, and that the elements of Fig. 7A represent droplets which are falling down between a guessed angle of ±45° with respect to a vertical line, the first module of VEL has to recognize automatically the two positions of each droplet. First the coordinates of the spot center points S and the vectorial distance $\bar{\mathbf{a}}$ between each two center points are calculated as illustrated in Fig. 7B. The vectorial distance $\bar{\mathbf{a}}$ can be split in a distance a and an angle β towards the vertical. Then a frequency analysis converts the spatial distribution of β into a normalized frequency distribution with the maximum F_{max} used as a norm. With the information of this preferential angle, a second frequency analysis with the distance **a** as the independent variable is carried out. The diagrams in Fig. 7 D and E show the two variables evaluated from Fig. 7A. The preferential angle β_p and the preferential distance $\mathbf{a}_p$ appear as peaks in the diagrams and form the mean velocity $\bar{\mathbf{v}}$.

This mean velocity is used by the second module of the subroutine VEL in order to find out the real droplet velocities. For this realization the magnitude $\mathbf{a}_p$ of $\bar{\mathbf{v}}$ is incremented by the tolerance $\pm 0.2\ \mathbf{a}_p$, and its corresponding angle β_p is also incremented by the tolerance $\pm\beta_0$. β_0 can be varied between 7 and 15° allowing for strong variations of the droplet trajectories. Figure 7C shows the result of applying the subroutine VEL on Fig. 7A. The scheme in Fig. 8 illustrates the working method of the second module of VEL. Herein V_i and β_i mean the real magnitude and direction of the velocity corresponding to the imaged positions of the droplet, respectively.

5. RESULTS AND DISCUSSION

5.1 Spray Characterization

The diagrams of Figs. 9A and 9B summarize, in form of arithmetic mean values of drop diameters and velocities, a great amount of data. The positions, sizes and velocities of about two million droplets were stored. The pressure p_v of the vapor environment is plotted as a parameter. The diagram of Fig. 9A exhibits an asymptotical decrease of the mean drop diameter $\bar{D}$ with increasing the liquid mass flow rate. The increase in the inertial forces, which depend on the

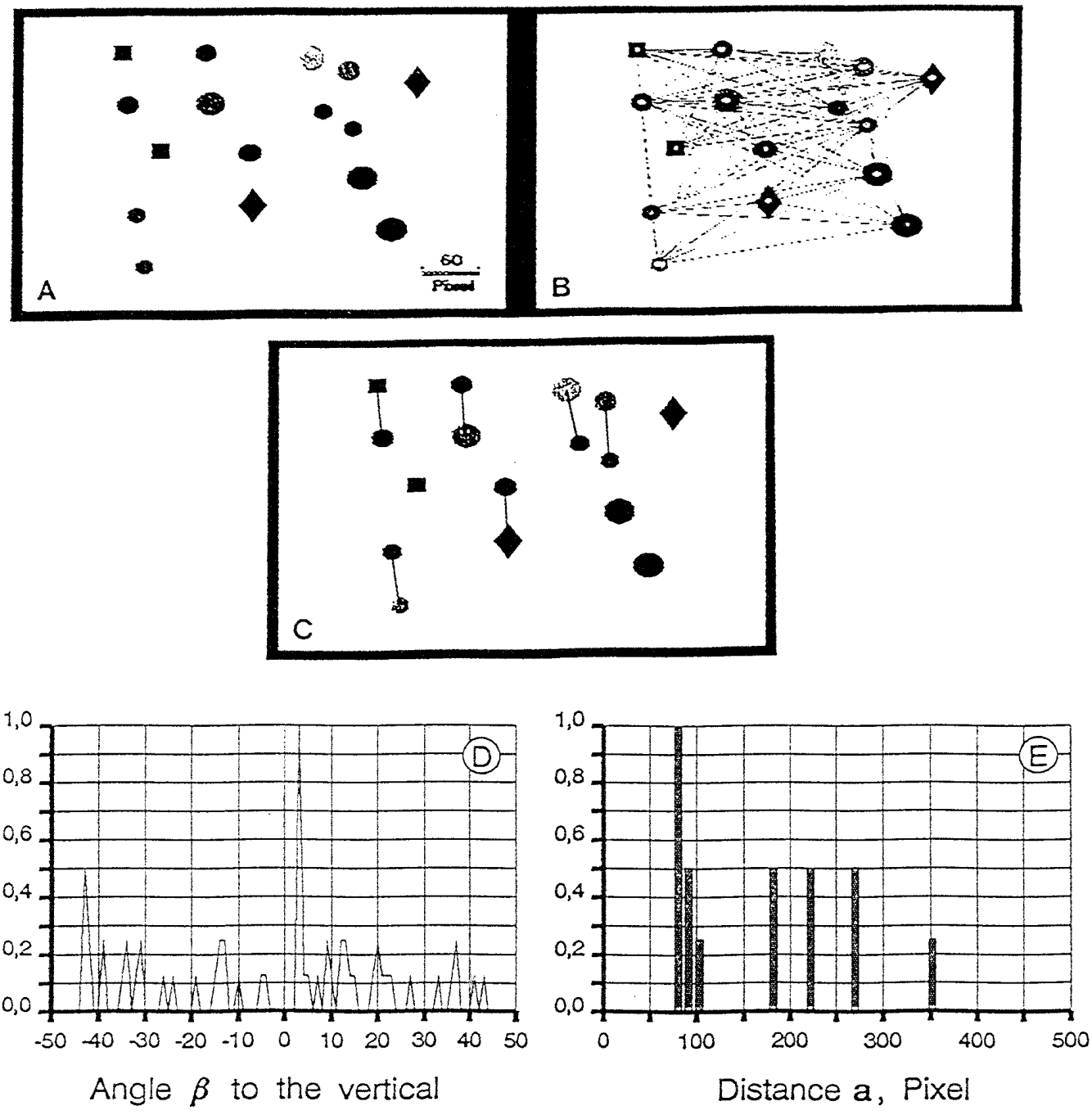

Figure 7: *Steps for recognition of spot couples corresponding to two successive positions of droplets using module 1 of the subroutine VEL. A) source image, B) calculation of the spot center points and velocity trajectories, C) identified couples, D) and E) Frequency analyses.*

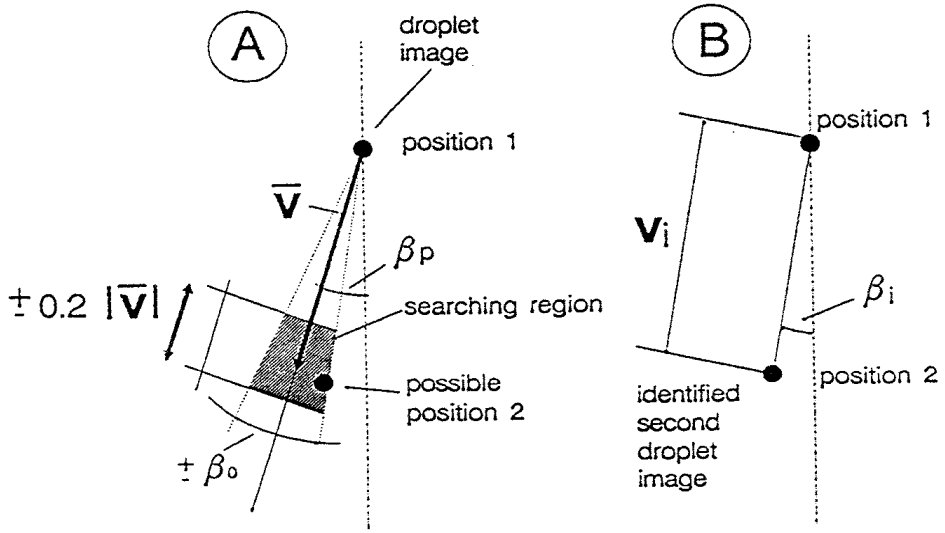

Figure 8: Operation of the second module of VEL.

flow rate, has a disintegrating effect upon the liquid sheet of the spray near the nozzle. This leads to the production of smaller droplets with a smaller diameter. A direct influence of the variation of the vapor pressure upon the drop size could not be found. Figure 9B reveals that the mean drop velocity grows almost linearly with increasing the liquid mass flow rate. In this case, the effect of varying the environmental pressure is obvious. The mean drop velocity diminishes when the vapor pressure increases as would be expected, since the vapor density and viscosity also increase when the saturation pressure of the vapor increases.

5.2 Condensation Rate and Heat Transfer Coefficient

The total condensation rate $\dot{M}_C$ on the spray can be expressed as the sum of the condensation rate on the injected liquid sheet, $\dot{M}_S$, and the condensation on the droplet swarm, $\dot{M}_D$. Thus,

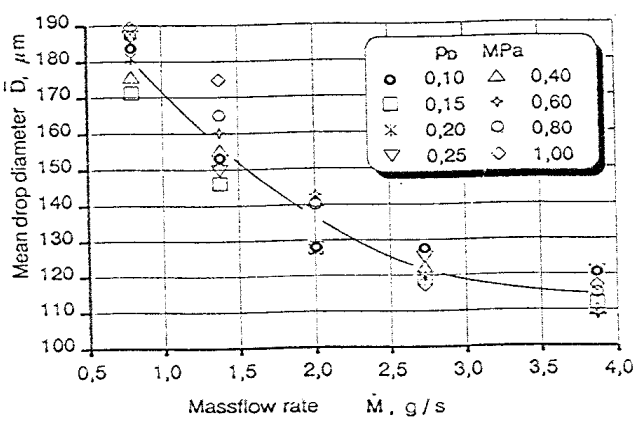

Figure 9A: Drop diameter

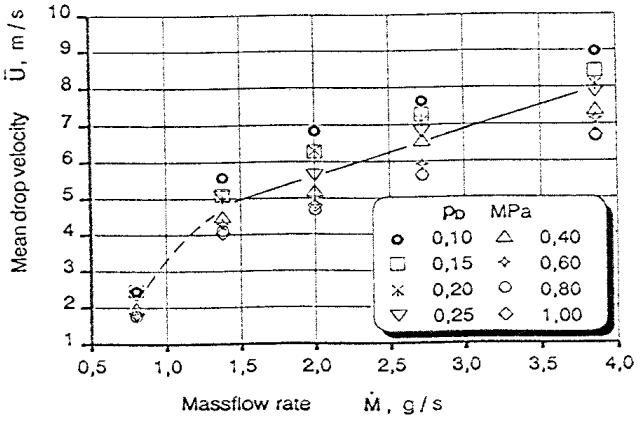

Figure 9B: Drop velocity

$$\dot{M}_C = \dot{M}_S + \dot{M}_D \tag{1}$$

with each evaluated separately. Only the condensation on the droplets is considered here.

Droplet growth rate: Applying the droplet measurement method of Fig. 5 to single pulsed holograms taken at two different distances from the spray nozzle, a mean droplet growth is obtained. For a given mass flow rate $\dot{M}$ and vapor pressure p_v, two holograms, the first one centered on z = 9 nozzle diameters and the second one on z = 96 nozzle diameters, were recorded and evaluated. A statistical comparison of the measured droplet classes allows for the evaluation of relative droplet size increments of the form

$$\delta\bar{D} = \left[\frac{F(D_i)}{F_{max}}\right]_f - \left[\frac{F(D_i)}{F_{max}}\right]_n \tag{2}$$

where D_i means the drop size class, $F(D_i)$ the frequency or repetition rate of drops of class D_i, F_{max} the maximum frequency, and the subindex f and n identify the far and the near spray regions, respectively. Typical measurements of the relative droplet growth $\delta\bar{D}$ in cumulative form ($\Sigma\,\delta D(D_i)$) are shown in Fig. 10. One observes a decrease of the curves under the zero-line followed by an increase above the zero-line. If the droplets are supposedly being in a growing process, more little drops are found in the n-region than in the f-region leading to a negative slope of the cumulative growing curves. The little drops in the n-region do not disappear; but wander to the next higher drop size class in the f-region. They increase $F(D_i) \mid_f$ with respect to $F(D_i) \mid_n$ so that the curves smoothly change to a positive slope, raise over the zero-line and keep positive.

The final value of the curves in Fig. 10 multiplied with the mean droplet diameter $\bar{D}$ represents the mean droplet growth $\delta\bar{D}$ and is equivalent to the integral

$$\delta\bar{D} = 2\int_0^\infty \dot{R}\,dt \tag{3}$$

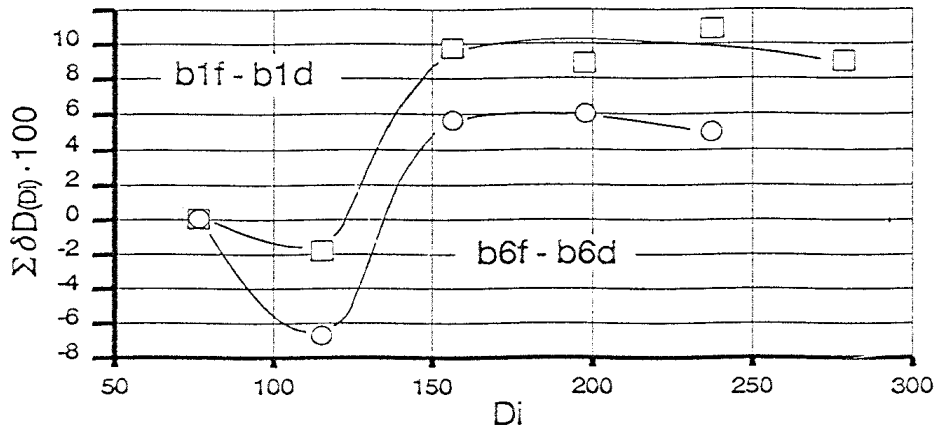

Figure 10: Relative droplet growth in a cumulative form.

Heat transfer on the droplets: Consider that (1) the emerging liquid from the conical sheet disperses as spherical droplets of diameter equal to the Sauter Mean Diameter D_{32}; (2) the temperature on the droplets surface is always equal to the vapor temperature T_{sat} and (3) the droplets reach a uniform temperature equal to the saturation temperature in an interval Δt, which can be expressed as a multiple of the time $\Delta t'$ needed by a liquid particle to go from the nozzle exit up to the break up point.

The condensation rate $\dot{M}_D$ on the droplet swarm is then given by

$$\dot{M}_D = \frac{\rho - \rho_v}{\rho} \frac{3(\delta\bar{D} + \delta\hat{D})}{D_{32}} (\dot{M} + \dot{M}_S) \tag{4}$$

with

$$\dot{M}_S = \frac{c_p[T_0 - T_{Lz}]}{h_{fg}} \dot{M} \tag{5}$$

where ρ_v means the density of the vapor, $\dot{M}$ the injected mass flow rate, $\dot{M}_S$ the condensed mass on the liquid sheet; $\delta\hat{D}$ is an idealized droplet growth corresponding to the liquid ligaments between the break up zone of the liquid sheet and the heat spray region (z = 9 nozzle diameters), and $\delta\bar{D}$ is the droplet growth between the near spray region (z = 9 nozzle diameters) and the far spray region (z = 96 nozzle diamters).

Now, $\dot{M}_{D,2}$ is given by

$$\dot{M}_{D,2} = \frac{\rho - \rho_v}{\rho} \frac{3(\delta\bar{D})}{D_{32}} (\dot{M} + \dot{M}_S + \dot{M}_{D,1}) \tag{6}$$

due only to $\delta\bar{D}$ between the center points z = 9 and z = 96 nozzle diameters, with which the temperature T(z = 9) is calculated.

Because of the assumption of total condensation at the center point of the far spray region (z = 96 nozzle diameters), it is possible to calculate the condensation rate $\dot{M}_{D,1}$, i.e. the condensation rate due to $\delta\hat{D}$. Assuming ideal condensation between $z = L_z$ and $z = 9$, $\dot{M}_{D,1}$ is given by:

$$\dot{M}_{D,1} = \frac{c_p[T_{z=9} - T_{Lz}]}{h_{fg}} (\dot{M} + \dot{M}_S) \tag{7}$$

from which $\delta\hat{D}$ can be calculated;

$$\delta\hat{D} = \frac{c_p[T_{z=9} - T_{Lz}]}{3h_{fg}} \cdot \frac{\rho}{\rho - \rho_v} \tag{8}$$

Equations (4) and (6) can be solved to give the condensation rate on the droplet swarm $\dot{M}_D$. The results of this evaluation are shown in Fig. 11A. The heat transfer coefficient h_D resulting from the vapor condensation on the droplets is obtained by applying the condition of continuity of heat flux at the interface between the droplets and their vapor environment, that is

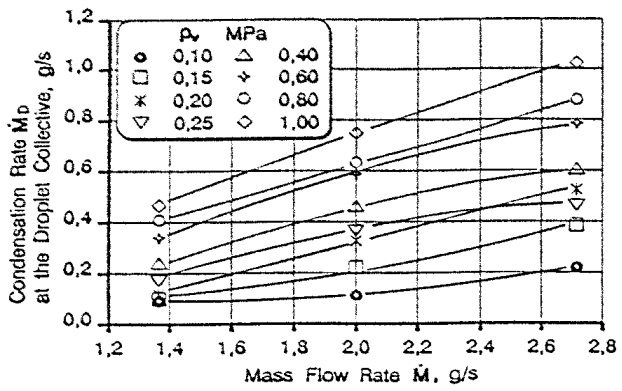

Figure 11A: Condensation rate.

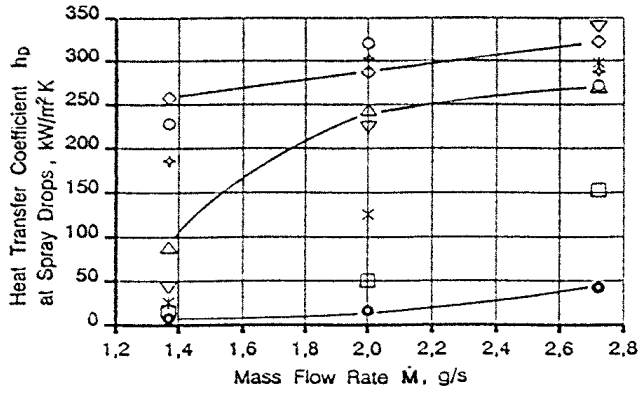

Figure 11B: Heat transfer coefficient.

$$h_D = \frac{h_{fg}\dot{M}_D}{N\pi(D_{32})^2\,[T_{sat}-T_{Lz}]} \tag{9}$$

where N is the number of drops

$$N = \frac{V_s}{\pi(D_{32})^2} \tag{10}$$

resulting from the liquid sheet volume V_S. In this case h_D varies between 5 and 325 kW/m²K. Figure 11B shows the behavior of the heat transfer coefficient as a function of the mass flow rate $\dot{M}$ at different vapor pressures p_v.

6. DISCUSSION

6.1 Uncertainty in the Evaluation of the Holograms

The main source of uncertainty in the measurement method lies in the pixel representation of circular objects (droplets), especially when these objects contain less than 10 pixels (independent of the absolute pixel size). By setting the resolution of the area measurement method to 5 pixels, a maximum error of ±3% was obtained by comparing a circular area with a pixel ensemble in which the amount of pixels was varied between 6 and 40 pixels. In this work, the smallest drop images contain 6 pixels (ϕ60 μm) and the largest ones 148 pixels (ϕ300 μm). For larger objects or structures, the error is less than 1%.

6.2 Uncertainty in the Heat Transfer Measurements

In this case the uncertainty is much higher than for the hologram evaluation. There are two major sources of error: (1) the statistical error E_S represented by the standard deviation being of the

order of 7%, and (2) the error E_T in the measurement of the bulk liquid temperature, which varies inversely proportional to the subcooling ΔT, from 5% at $\Delta T > 20°K$ up to 30% at $\Delta T \approx 1°K$.

The statistical error affects the measurement of the droplet growth directly, i.e. the heat transfer to the droplets. The temperature measuring error also affects the measurement of the heat transfer in both spray zones, the maximum relative error E_{max} in the condensation rate and the evaluation of the heat transfer coefficient.

7. CONCLUSIONS

The presented results suggest that the injection of subcooled liquids, through pressure–swirl nozzles, into a saturated vapor atmosphere at increased pressures leads to completely different dimensions than those reported at a low vapor pressure. The pressure influences not only the behavior of the injection spray, but also the heat and mass transfer associated with condensation: The heat transfer increases no longer with increasing the liquid velocity. Instead, it approximates asymptotically to its maximum value. Therefore, the design of injection facilities for work at high vapor pressures has to take into account the effect of the high pressure on the dynamics of the fluid flow and on the direct–contact condensation.

REFERENCES

1. Lekic, A. and Ford, J.D., Direct contact condensation on a spray of subcooled liquid droplets, *Int. J. Heat & Mass Trans.* 23: 1531–1537, 1980.
2. Lee, S.Y. and Tankin, R.S., Study of liquid spray (water) in a condensable environment (steam), *Int. J. Heat & Mass Tran.* 27(3): 363–374, 1984.
3. Hijikata, K., Mori, Y. and Kawaguchi, S., Direct contact condensation of vapour on falling droplets, *Int. J. Heat & Mass Trans.* 27: 1631–1640, 1984.
4. Celata, G.P., Cumo, M., D'Annivale and Farello, G.E., Direct contact condensation of steam on droplets, *Int. J. Multiphase Flow* 17(2): 191–211, 1991.
5. Trollinger, J.D., 1975), Particle field holography, *Optical Eng.* 14: 470–481.
6. Chávez, A. and Mayinger, F., Single– and double pulsed holography for the characterization of sprays of refrigerant R113 injected into its own saturated vapor, In: *Experimental Heat Transfer*, Fluid Mechanics and Thermodynamics, R.K. Shah, E.N. Ganic and K.T. Yang (eds.), Elsevier, pp. 848–854, 1988.